

# Interaction and temperature effects on the magneto-optical conductivity of Weyl liquids

S. Acheche, R. Nourafkan, J. Padayasi, N. Martin, and A.-M. S. Tremblay  
*Département de physique, Institut quantique, and Regroupement québécois sur les matériaux de pointe, Université de Sherbrooke, Sherbrooke, Québec, Canada J1K 2R1*

(Dated: July 29, 2020)

Negative magnetoresistance is one of the manifestations of the chiral anomaly in Weyl semimetals. The magneto-optical conductivity also shows transitions between Landau levels that are not spaced as in an ordinary electron gas. How are such topological properties modified by interactions and temperature? We answer this question by studying a lattice model of Weyl semimetals with an on-site Hubbard interaction. Such an interacting Weyl semimetal, dubbed as Weyl liquid, may be realized in  $\text{Mn}_3\text{Sn}$ . We solve that model with single-site dynamical mean-field theory. We find that in a Weyl liquid, quasiparticles can be characterized by a quasiparticle spectral weight  $Z$ , although their lifetime increases much more rapidly as frequency approaches zero than in an ordinary Fermi liquid. The negative magnetoresistance still exists, even though the slope of the linear dependence of the DC conductivity with respect to the magnetic field is decreased by the interaction. At elevated temperatures, a Weyl liquid crosses over to bad metallic behavior where the Drude peak becomes flat and featureless. We comment on the effect of a Zeeman term.

## I. INTRODUCTION

Weyl semimetals are three-dimensional (3D) analogs of graphene with topologically protected band crossings and interesting transport phenomena. Monopnictides TaAs, TaP, NbAs and NbP are prime examples<sup>1-3</sup>. In the presence of a uniform magnetic field, a Weyl node splits into degenerate Landau levels with a chiral zeroth level that crosses the Fermi level and gives a non-zero DC conductivity. The degeneracy of the zeroth Landau level depends on the amplitude of the magnetic field. Hence, the resistivity in the presence of parallel electric and magnetic fields acquires a magnetic-field-dependent contribution, the so-called chiral anomaly contribution, which is negative in contrast with the conventional metal.<sup>4</sup> Negative magnetoresistance has been experimentally observed in Weyl semimetals such as TaAs<sup>5,6</sup> or  $\text{Mn}_3\text{Sn}$ <sup>7</sup> even though it is not always clear whether its origin is the chiral anomaly.<sup>8-10</sup>

The standard Drude contribution and the chiral-anomaly contribution compete with each other in general, leading to a nonmonotonic dependence of the conductivity (or resistivity) on magnetic field. Whether the chiral anomaly-related conductivity dominates or not depends on the ratio of different scattering times, such as inter-Weyl point scattering time and transport scattering time and the location of the chemical potential with respect to Weyl points. These quantities are impacted by both temperature and electron-electron interaction, in particular in correlated Weyl semimetals such as  $\text{Mn}_3\text{Sn}$ <sup>7</sup>, raising the question of their influence on the magnetoresistance of Weyl semimetals.

The frequency dependence of the conductivity in Weyl semi-metals also has interesting features. At zero temperature and in the absence of a magnetic field, the optical conductivity in the continuum limit and without interactions exhibits a linear frequency dependence with vanishing DC limit when the chemical potential is at the

nodes.<sup>11,12</sup> This is a consequence of the parabolic density of states. It has been observed in the low-temperature, low-frequency optical spectroscopy of the known Weyl semimetal TaAs.<sup>13</sup> Adding a magnetic field, not only leads to the above-mentioned chiral-anomaly in the DC conductivity, it modifies the optical conductivity that now consists of a narrow low-frequency peak, whose DC value manifests the chiral anomaly, and of a series of asymmetric peaks from interband transitions superimposed on the linear background from the no-field case<sup>11,14</sup>. The case of hybridized Weyl nodes has also been considered both theoretically and experimentally for NbP<sup>15</sup>. The effect of long-range Coulomb interactions on interband magneto-optical absorption has been studied theoretically using GRPA<sup>16</sup>.

Here, using dynamical mean-field theory<sup>17</sup>, we study, based on Ref. 18, the effects of both local Hubbard-type interactions and temperature on the magneto-optical conductivity. We show how interactions and temperature broaden the low-frequency peak, renormalize and redistribute optical spectral weight between the low-frequency peak and the inter-band transitions between Landau levels and how interactions transfer optical weight to the high-frequency incoherent satellites. Theoretically, all this is related to the robustness of the quasiparticle picture, which we thoroughly analyze. We will refer to the interacting Weyl semimetal as a Weyl liquid<sup>19</sup>, by analogy with the Fermi liquid.

We also investigate the temperature-induced transition to bad-metal behavior. This occurs as follows in normal metals. The half bandwidth of the low-frequency peak in optical spectra, proportional to the scattering rate, grows with increasing temperature because of thermally induced scattering events grow. Upon approaching the so-called Mott-Ioffe-Regel<sup>20</sup>, the scattering rate becomes of the order of the bandwidth, and the low-frequency peak becomes flat and essentially featureless<sup>21-24</sup>. Quasiparticles and Fermi liquid behavior disappear. How this

physics manifests itself in a Weyl liquid is another subject of this study.

After we introduce the model in Sec. II, we show the effect of interactions on single-particle properties in Sec. III and then of interactions and temperature on the conductivity in Sec. IV. Appendix A shows that the Zeeman term has little influence on the magneto-optical conductivity, even though it shifts the Landau levels. Appendix B contains a perturbative estimate of the imaginary part of the self-energy, and shows that despite its  $\omega^8$  dependence, the usual quasiparticle renormalization  $Z$  follows. Appendix C explains how to extract the weight of an isolated Drude peak directly from imaginary frequency.

## II. MODEL AND METHODS

We start from a Weyl semimetal model defined on a cubic lattice and add a particle-hole symmetric Hubbard interaction. In the zero-field case, it reads

$$\hat{H} = \hat{H}_0 + U \sum_{\mathbf{r}} (\hat{n}_{\mathbf{r}\uparrow} - 1/2)(\hat{n}_{\mathbf{r}\downarrow} - 1/2) - \mu \sum_{\mathbf{r}} \hat{n}_{\mathbf{r}} \quad (1)$$

where  $U$  is the strength of the Hubbard interaction,  $\hat{n}_{\mathbf{r}\uparrow}$  ( $\hat{n}_{\mathbf{r}\downarrow}$ ) are occupation numbers for spin up (down), and  $\mu$  is the chemical potential. The non-interacting Hamiltonian  $\hat{H}_0$  in second quantized form is<sup>25</sup>

$$\begin{aligned} \hat{H}_0 = & \sum_{\mathbf{k}} \hat{\mathbf{C}}_{\mathbf{k}}^\dagger [-(2t \cos k_x + 2t \cos k_y + 2t_z \cos k_z) \sigma_z \\ & + (2t \sin k_y) \sigma_y + (2t \sin k_x) \sigma_x] \hat{\mathbf{C}}_{\mathbf{k}}, \end{aligned} \quad (2)$$

where  $t$  and  $t_z$  are independent parameters and  $\sigma_x$ ,  $\sigma_y$  and  $\sigma_z$  represent Pauli matrices. The Hamiltonian is written in spin-space, so the creation and annihilation operators are two-spinors,  $\hat{\mathbf{C}}_{\mathbf{k}} = (\hat{c}_{\mathbf{k},\uparrow}, \hat{c}_{\mathbf{k},\downarrow})$ . We also take Boltzman's constant  $k_B$  equal to unity and  $t = t_z = 1$  for all calculations and use units where  $\hbar = 1, e = 1$ . In addition, the lattice constant  $a$  equals unity. In this regime,  $t = t_z$ , there are four Weyl nodes in the first Brillouin zone of the non-interacting Hamiltonian located at  $(0, \pi, \pm\pi/2)$  and  $(\pi, 0, \pm\pi/2)$ . Time-reversal symmetry is broken, but this model has other symmetries detailed in Ref. 26.

We introduce the orbital effects of a uniform magnetic field through the Peierls substitution<sup>27</sup>. The magnetic Hamiltonian (in the tight-binding form) then includes a site-dependent Peierls phase  $\phi_{nm}(B)$  that changes the symmetries of the model. What about a Zeeman term? When the Pauli matrices act on spin, there is a Zeeman term whose effect on the Hamiltonian has been discussed in Ref. 26. In Appendix A we show that in the non-interacting case the Zeeman term influences the magneto-optical spectrum only when lattice effects are important and we show that the effects are very small. The Landau wave functions are a combination of up and down

spins and in the continuum limit, the Zeeman term simply shifts the position of the Weyl nodes and does not influence the spectrum at all. So from now on, we do not include a Zeeman term. We pick magnetic field values commensurate with the original lattice, namely we take  $eBa^2/h = p/q$  with rational values of  $p/q$ <sup>28</sup>. In the rest of this paper, and with no loss of generality, we set  $p = 1$ . The applied magnetic field is in the  $z$ -direction and we use the Landau gauge (*i.e.* a vector potential  $\mathbf{A} = (0, Bx, 0)$ ) to preserve translation symmetry along the  $y$ -direction. This leads to the following Harper matrix:

$$\mathbf{H}_H = \begin{pmatrix} \mathbf{H}_{\uparrow\uparrow} & \mathbf{H}_{\uparrow\downarrow} \\ \mathbf{H}_{\downarrow\uparrow} & \mathbf{H}_{\downarrow\downarrow} \end{pmatrix}. \quad (3)$$

Each of the sub-matrices in the above equation is of dimension  $q \times q$ . They are defined as follows,

$$\mathbf{H}_{\uparrow\uparrow} = \begin{pmatrix} M_0 & -t & 0 & \dots & -t \\ -t & M_1 & -t & \dots & 0 \\ 0 & \ddots & \ddots & \ddots & \vdots \\ -t & 0 & \dots & -t & M_{q-1} \end{pmatrix}, \quad (4a)$$

$$\mathbf{H}_{\uparrow\downarrow} = \begin{pmatrix} A_0 & -it & 0 & \dots & it \\ it & A_1 & -it & \dots & 0 \\ 0 & \ddots & \ddots & \ddots & \vdots \\ -it & 0 & \dots & it & A_{q-1} \end{pmatrix}, \quad (4b)$$

with

$$\mathbf{H}_{\downarrow\uparrow} = \mathbf{H}_{\uparrow\downarrow}^\dagger, \quad \mathbf{H}_{\downarrow\downarrow} = -\mathbf{H}_{\uparrow\uparrow}, \quad (5)$$

and with the definitions  $M_n = -2t \cos(k_y + 2\pi np/q) - 2t_z \cos k_z$  and  $A_n = 2it \sin(k_y + 2\pi np/q)$ .

Equation 3 describes a magnetic unit cell with  $q$  sites in the  $x$  direction. The full Hamiltonian includes a periodic extension of Harper matrix along the  $x$  axis, the chemical potential and the Hubbard interaction. For the values of  $q$  that we choose, the Harper matrix is sufficiently large and the corresponding reduced Brillouin zone along the  $k_x$  direction sufficiently small that dependencies on  $k_x$  can be neglected. These dependencies are associated with the periodicity of the magnetic unit cell and they become important in the large field limit where the magnetic unit cell has only a few sites. Consequently, the sites inside the magnetic unit cell have identical local density of states (spin up + spin down) at half-filling. Therefore, we are in the Landau regime defined in Ref. 29.

In this approximation, the free Hamiltonian that takes maximum advantage of translational invariance is

$$\hat{H}_0 = \sum_{k_y, k_z} \hat{\mathbf{C}}^\dagger \mathbf{H}_H \hat{\mathbf{C}} - \mu \sum_i \hat{n}_i \quad (6)$$

where the creation and destruction operators are defined in the basis:  $\hat{\mathbf{C}} = (\hat{c}_{1,k_y,k_z,\uparrow}, \dots, \hat{c}_{q,k_y,k_z,\downarrow})$ .

We solve the interacting Hamiltonian non-perturbatively using the Dynamical Mean Field Theory (DMFT) framework<sup>17</sup>. The expected correction to the DMFT self-energy<sup>30</sup> is an additive static momentum dependent self-energy that would renormalize the energy dispersion and lead to corresponding vertex corrections. These static corrections should not be important when long-wavelength spin fluctuations are absent. Ref. 29 contains the derivation of the DMFT equations that include the orbital effects of a uniform magnetic field. In summary, the local self-energy depends on the magnetic field and the self-consistency equation itself is unaltered. The effect of the magnetic field on the self-energy comes from the non interacting density of states of the Landau levels and the self-consistency equation.<sup>29,31</sup>

We use an exact diagonalisation (ED) impurity solver for the impurity problem with a finite number of bath sites,  $n_b$ .<sup>32,33</sup> Though still of considerable size, the  $n_b = 5$  orbital Hamiltonian in this scheme can be diagonalized exactly to compute the local Green's function at finite temperature.

### III. MAGNETIC FIELD AND ELECTRONIC INTERACTION EFFECTS ON SINGLE-PARTICLE PROPERTIES

We first consider the effects of magnetic field and interactions on the density of states and then discuss the self-energy. This leads us to comment on the resilience of quasiparticles in the presence of interactions in a Weyl semimetal.

#### A. Density of states

For a non-interacting Weyl semimetal without magnetic field, described by Eq. 2, the density of states at low energy is characterized by  $\omega^2$  behavior, with a vanishing density of states at  $\omega = 0$ . With a magnetic field, a finite field-dependent density of states appears at low energies as shown in Fig. 1a. The non-interacting density of states in this figure is obtained from

$$\rho(\omega) = \frac{1}{N} \sum_n \int \frac{dk_y dk_z}{(2\pi)^2} \delta(\epsilon_{n,k_y,k_z} - \omega) \quad (7)$$

where  $N$  is the total number of Landau levels,  $n$  is the Landau level index and  $\epsilon_{n,k_y,k_z}$  the corresponding dispersion energy obtained from the Harper Matrix. The finite field-dependent density of states at low energy increases with increasing field. Apart from this, a magnetic field does not influence the main characteristics and the bandwidth of the density of states of a non-interacting Weyl semimetal.

Fig. 1a also shows the density of states of the interacting system. Apart from the lower and upper Hubbard

bands (incoherent satellites around  $\omega = \pm 10$  on Fig. 1a), the interaction tends to shrink the coherent quasiparticle bandwidth by the quasiparticle weight  $Z$ . However, the density of states at the Fermi level is not affected by electronic correlations. This can be explained as follows. Physically, the spectral function is proportional to the quasiparticle weight  $Z$ , but the one-dimensional density of states of the chiral level is proportional to one over the renormalized Fermi velocity  $Zv_F$  so that the two factors of  $Z$  cancel each other. The density of states for chiral Landau levels in the quasiparticle approximation is then given by

$$\rho(\omega) \propto \frac{\Theta [Z^{-1}(\omega/v_F) + k_c] - \Theta [Z^{-1}(\omega/v_F) - k_c]}{|v_F|}, \quad (8)$$

where  $v_F$  stands for the Fermi velocity,  $k_c$  is an energy cut-off and  $\Theta$  is the step function. Equation 8 shows that the density of states is insensitive to the quasiparticle spectral weight  $Z$ , but the range of frequencies where it applies is narrowed down. There is another way to explain that the density of states at the Fermi level is independent of interactions: It is a general property of single-site DMFT at low enough temperature. Indeed, one can show, using Luttinger's theorem for a momentum-independent self-energy<sup>34</sup>, that the density of states at the Fermi level ( $\omega = 0$ ) is independent of interactions. One has to assume that this remains valid for a range of energies close to the Fermi level.

#### B. Self-energy

The scattering amplitude is related to the imaginary part of the self-energy, which depends on  $U$ . At fixed  $U$ , we investigate the effect of the magnetic field on the imaginary part of the self-energy at low temperature (corresponding to an inverse temperature  $\beta = 80$ ) by comparing the case without a magnetic field, *i.e.*  $B = 0$ , with the case where  $B = 2\pi/40$ , and with the case where  $B = 2\pi/16$ , *i.e.* in the quantum limit. The latter is characterized by a clear separation between the zeroth and the first non-zero Landau levels.

Figure 1b illustrates the effect of magnetic field on the imaginary part of the self-energy for the first few Matsubara frequencies at  $\beta = 80$ ,  $U = 12$  and half-filling. As in the case of the Hubbard model on the square lattice<sup>26</sup>, the magnetic field does not have a large effect on the self-energy. For  $B = 2\pi/40$ , there are few differences with the self-energy without a magnetic field. However, for  $B = 2\pi/16$  we can clearly see that the self-energies depart from each other at larger Matsubara frequencies.

Those differences at intermediate frequencies come from the significant modification of the local density of states due to the orbital effect of the magnetic field. It is also interesting to note that despite these differences, the three self-energies have the same value at the first Matsubara frequency. This indicates that the scattering

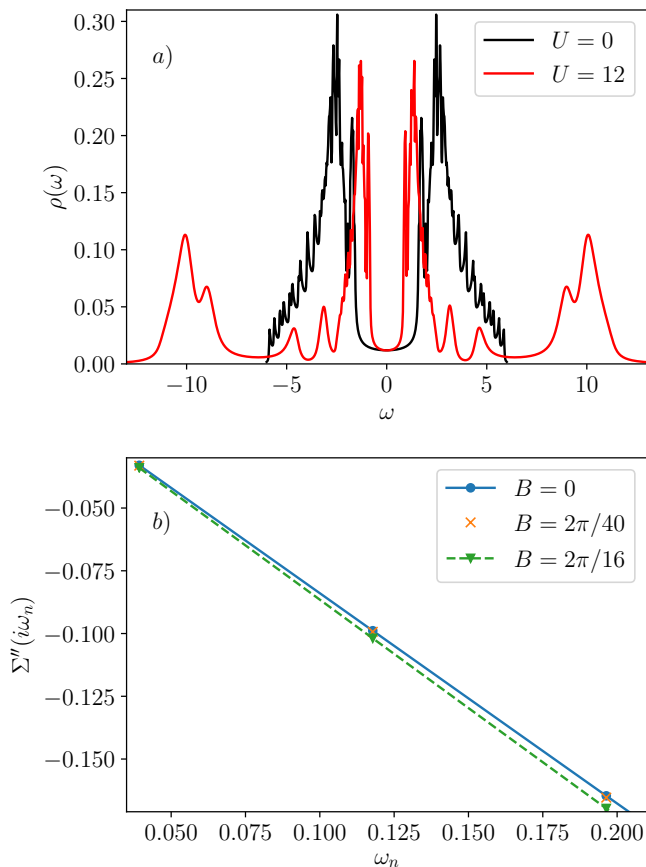


Figure 1. (color online) a) Local density of states for non-interacting (black line) and interacting (continuous red line) Weyl semimetals in the presence of an external magnetic field ( $B = 2\pi/16$ ). A Lorentzian broadening  $\eta = 0.01$  has been used for both plots. Features that are sharper than 0.01 in frequency then, cannot be resolved. Note that the flat part of the spectrum near  $\omega = 0$  is insensitive to a wide range of values of  $\eta$  since smoothing the density of states when it is already frequency independent does not change anything. b) Imaginary part of the self-energy at the three lowest Matsubara frequencies for the case without a magnetic field, *i.e.*  $B = 0$ , the case where  $B = 2\pi/40$ , and finally in the quantum limit where  $B = 2\pi/16$ . The inverse temperature is  $\beta = 80$ .

times at the Fermi level for half-filling are essentially the same with or without magnetic field.

### C. Resilience of quasiparticles

Although it is not completely apparent from the above results, quasiparticles are remarkably resilient in a Weyl semimetal. To show this, let us momentarily remove the magnetic field. At small interaction strength, the self-energy can be calculated with the iterated perturbation theory (IPT) solver<sup>35</sup> but without the DMFT self-consistency. Then one can use the quadratic effective density of state of Weyl semimetals near the Fermi energy and obtain analytically the imaginary part of the

self-energy at low frequency for a single Weyl node (see the derivation in Appendix B):

$$\Sigma''(\omega) \propto -\frac{U^2\omega^8}{\pi^5 v_F^9}, \quad (9)$$

where  $v_F$  is the Fermi velocity. Nevertheless, one expects that since this suggests the existence of quasiparticles, this result should be valid for larger values of  $U$ . Note that this unusual behavior is very different from Fermi liquid theory where  $\Sigma''(\omega)$  is quadratic in frequency. From the point of view of lifetime, the “Weyl liquid” seems to lead to even more stable quasiparticles than Fermi liquids.

But what about the quasiparticle spectral weight  $Z$ ? Appendix B shows that there is a finite value of  $Z$  and calculations show that, as expected, it decreases (roughly as  $-U^2$ ) as  $U$  increases. The smallness of the imaginary part of the self-energy at low frequency offers a clue for the robustness of quasiparticle physics. This justifies a quasiparticle approach where the main effect of the interactions is encoded in the quasiparticle weight with an (extremely) small lifetime for the quasiparticles. However, the above derivation is only valid in the absence of magnetic field since it relies on a vanishing density of states at the Fermi level. When an external magnetic field is applied, a finite density of states appears and that could change the physics.

## IV. CONDUCTIVITY OF INTERACTING WEYL SEMIMETALS

In this section, we use our knowledge of single-particle properties to compute the optical conductivity and find out how it is affected by magnetic field, temperature and finite bandwidth.

Let us first consider the current-current correlation function in Matsubara frequency. In linear response theory at zero momentum and neglecting vertex corrections, this correlation function  $\Pi_{zz}(\mathbf{q} \rightarrow 0, i\nu_n)$  along the  $z$  direction is<sup>36,37</sup>

$$\begin{aligned} \Pi_{zz}(i\nu_n) = & -\frac{\pi}{N\beta} \sum_{\mathbf{k}\omega_m} \text{Tr} \left[ \mathbf{a}_{zz}(\mathbf{k}) \mathbf{G}(\mathbf{k}, i\omega_m) \right. \\ & \left. - \mathbf{v}_z(\mathbf{k}) \mathbf{G}(\mathbf{k}, i\omega_m + i\nu_n) \mathbf{v}_z(\mathbf{k}) \mathbf{G}(\mathbf{k}, i\omega_m) \right], \end{aligned} \quad (10)$$

where  $\beta = 1/(k_B T)$  is the inverse of temperature,  $i\omega_n$  is the fermionic Matsubara frequency,  $\text{Tr}$  is the trace over  $2q \times 2q$  matrices,  $\mathbf{a}_{zz}(\mathbf{k}) = \partial_{k_z}^2 \mathbf{H}_H$  is the inverse effective mass tensor,  $\mathbf{v}_z(\mathbf{k}) = \partial_{k_z} \mathbf{H}_H$  the velocity matrix along the  $z$  direction, and  $\mathbf{G}(\mathbf{k}, i\omega_m)$  is the interacting Matsubara Green function.  $\Pi_{zz}$  is composed of two parts:  $\Pi^{Dia}$ , the diamagnetic part and  $\Pi^{Para}$ , the paramagnetic part (respectively, first and second term in Eq. 10). Gauge invariance imposes that these two parts cancel each other

perfectly at  $\nu_n = 0$ . After analytic continuation, the real part of the retarded conductivity  $\sigma'_{zz}$  is

$$\sigma'_{zz}(\omega) = \frac{\Pi''_{zz}(\omega)}{\omega}, \quad (11)$$

where  $\Pi''_{zz}(\omega)$  is the imaginary part of  $\Pi_{zz}(\omega)$ . One can also compute the real part of conductivity directly in real frequency from<sup>38</sup>

$$\sigma'_{zz}(\omega) = \frac{\pi}{N} \sum_{\mathbf{k}} \int d\epsilon \text{Tr} \left[ \mathbf{v}_z(\mathbf{k}) \mathbf{A}(\mathbf{k}, \epsilon) \mathbf{v}_z(\mathbf{k}) \mathbf{A}(\mathbf{k}, \omega + \epsilon) \right] \times \frac{f(\epsilon) - f(\omega + \epsilon)}{\omega}, \quad (12)$$

where  $\mathbf{A}$  is the spectral function matrix and  $f$  is the Fermi-Dirac distribution function. In the DC limit, the difference of the Fermi-Dirac distribution functions in Eq. 12 can be replaced by the derivative with respect to frequency at  $\omega = 0$ . Equation 12 is valid only when the trace is real, otherwise, additional terms coming from the paramagnetic term of the current-current correlation function have to be taken into account to obtain the real part of the conductivity. Moreover, since the system breaks time-reversal symmetry, the spectral weight must be computed from the anti-hermitian part of the Green's function matrix

$$\mathbf{A}(\mathbf{k}, \omega) = \frac{1}{2i\pi} [\mathbf{G}^\dagger(\mathbf{k}, \omega) - \mathbf{G}(\mathbf{k}, \omega)], \quad (13)$$

where the spectral weight is normalized as follows,  $\int d\omega \mathbf{A}(\mathbf{k}, \omega) = \mathbf{1}$ . The real-frequency dependent Green's functions are obtained by analytic continuation using the Padé approximant method<sup>39</sup> with a Lorentzian broadening  $\eta = 0.01$ .

### A. Interaction effects in the low-temperature limit

Figure 2 shows the magneto-optical conductivity of the interacting Weyl semimetal for several interaction strengths and  $B = 2\pi/16$ . It is an even function of frequency. In the presence of Hubbard interactions, the magneto-optical conductivity has three well defined features: The Drude Peak near zero frequency, the interband transitions between Landau levels<sup>11</sup> and incoherent peaks that are a consequence of Hubbard bands in the density of states. The interband transitions at lower frequency are quite similar to the results obtained from a non-interacting continuum model of Weyl nodes<sup>11</sup>, *i.e.* a series of asymmetric peaks superimposed on the linear background from the no-field case. In our case, the lattice introduces a natural cutoff and differences with the continuum model at higher energy.

The three parts of the optical conductivity are affected differently by the Hubbard interaction. It is the chiral zero'th Landau level that leads to a finite density of states at the Fermi level and to a Drude peak in the

optical conductivity.<sup>4,40</sup> Upon increasing  $U$ , the Drude peak decreases in intensity and in weight because of the quasiparticle weight  $Z$ , even if the density of state at  $\omega = 0$  is not affected by electron-electron interactions. The optical spectral weight of the interband contribution is also reduced by interaction and the optical weight is transferred to the incoherent satellite at high energy. Furthermore, the optical gap between low-frequency peak and the interband contribution is decreased by the interaction, as can be seen from Fig. 2a.

A quantitative study of the Drude peak in real frequency is cumbersome since it requires analytic continuation of numerical data. This could introduce artifacts, especially in presence of interactions. Fortunately, at low temperatures the weight of the Drude peak can be extracted from the Matsubara-frequency current-current correlation function  $\Pi_{zz}^{Para}(i\nu_n)$ . As shown in Fig. 2b,  $\Pi_{zz}^{Para}(i\nu_n)$  is a smooth function of the Matsubara frequencies except at the lowest frequency, *i.e.*,  $\nu_0 = 0$ . The sudden increase at this frequency indicates a non-zero DC conductivity. Indeed, in an insulator,  $\Pi_{zz}^{Para}(i\nu_n)$  smoothly reaches its zero frequency value as one can see from  $B = 0$  result. Furthermore, in the interacting Weyl semimetals at low temperatures, the Drude peak is separated from the rest of the optical spectrum by a clear gap (see Fig. 2a). This allows us to show that the jump in  $\Pi_{zz}^{Para}(i\nu_n)$  at the lowest frequency scales with the Drude peak weight. The details of the derivation are presented in Appendix C.

With the help of Eq. C5, we are able to follow the fate of the Drude weight,  $W_D = \int d\omega \sigma^D(\omega)$ , with and without interaction. Here, we define  $\sigma'_{zz}(\omega) = \sigma_{zz}^D(\omega) + \sigma^{res}(\omega)$  because the Drude peak is separated with an energy gap from the rest of the optical spectrum. As one can see from Fig. 3a, at low temperatures the interaction dependence of the low-frequency peak weight normalized by the non-interacting one follows exactly the quasiparticle weight for all values of  $U$  tested. The normalized Drude weight scales like the quasiparticle weight  $Z$ , even near the Mott transition<sup>41</sup> (around  $U = 20$ ), a clear sign of the robustness of quasiparticle physics.

The shrinking of interband contributions with increasing  $U$  is also a sign of quasiparticle physics. Indeed, the quasiparticle weight  $Z$  renormalizes the whole band, so the Landau levels become closer to each other. This leads to excitations at lower frequency than in the absence of interactions. Contrary to interband transitions, transitions between incoherent Hubbard bands and quasiparticle bands and between the lower and the upper Hubbard bands is due to the frequency dependence of the self-energy and cannot be explained by the quasiparticle spectral weight alone. However,  $Z$  still governs a large part of the optical conductivity.

In Fig. 3b, we present  $W_{res} = \int d\omega \sigma^{res}(\omega)$  normalized by its value at  $U = 0$ . This quantity is easily computed with the help of Eq. C5 and of

$$W_{res} = \int_{-\infty}^{+\infty} d\omega \sigma^{res}(\omega) = \tilde{\Pi}_{zz}^{Para}(i\nu_n = 0), \quad (14)$$

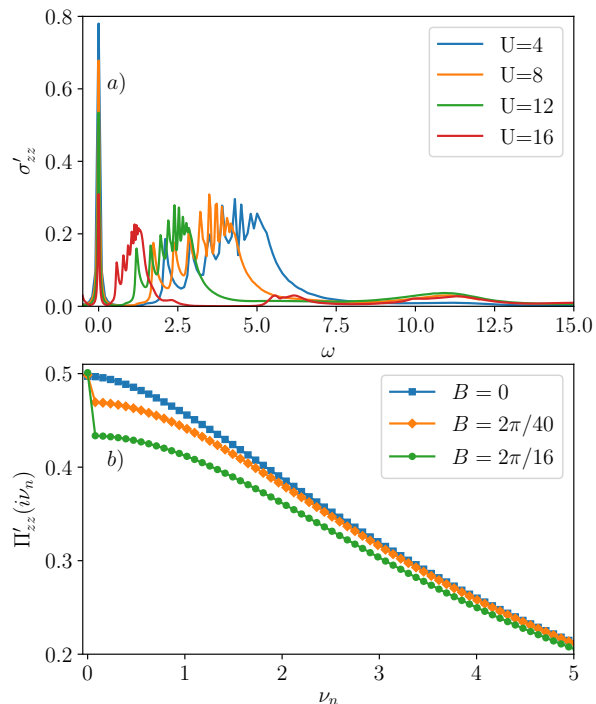


Figure 2. (color online) a) Magneto-optical conductivity of the interacting Weyl semimetal in an external magnetic field for several interaction strengths and  $\beta = 80$ . b) Magneto-optical polarization as a function of bosonic Matsubara frequency for  $B = 2\pi/16$ ,  $B = 2\pi/40$  and  $B = 0$ , (*i.e.* without external magnetic field in the latter case). DC conductivity scales with the jump at the lowest frequency. The figure shows that DC conductivity (resistivity) is increasing (decreasing) upon increasing field, *i.e.*, reducing  $q$ .

where  $\tilde{\Pi}_{zz}^{Para}$  denotes the paramagnetic part of the current-current correlation function without the jump at the lowest frequency. It can be obtained from an extrapolation to  $\nu_n = 0$  of a polynomial fit of  $\Pi_{zz}^{Para}(i\nu_n \neq 0)$ .

In the weak to intermediate range of interaction,  $W_{res}$  depends only weakly on the interaction strength. For interaction strengths larger than the bare band-width,  $W_{res}$  decreases at a faster rate and eventually saturates to a finite value when the system undergoes a phase transition to a Mott insulator. Hence the variation of  $W_D$  or of the effective mass with interaction is more pronounced than the variation of  $W_{res}$ .

Figure 3c shows the normalized  $W_{res}$  as a function of square root of the quasiparticle weight  $\sqrt{Z}$ . The point at  $Z = 0$  is in the insulator. The linearity of the curve and the value of the slope, equal to  $1/2$  over the whole range, except for the transition from metal to insulator, indicates that the ratio is directly proportional to the square root of  $Z$ . We have not found a simple argument for this result.

Finally, consider the magnetoresistance of a Weyl liquid. For the values of  $q$  tested in this paper ( $q \in [16, 100]$ ), the Drude weight increases linearly with the magnetic field (see figure 4). This is the famous negative

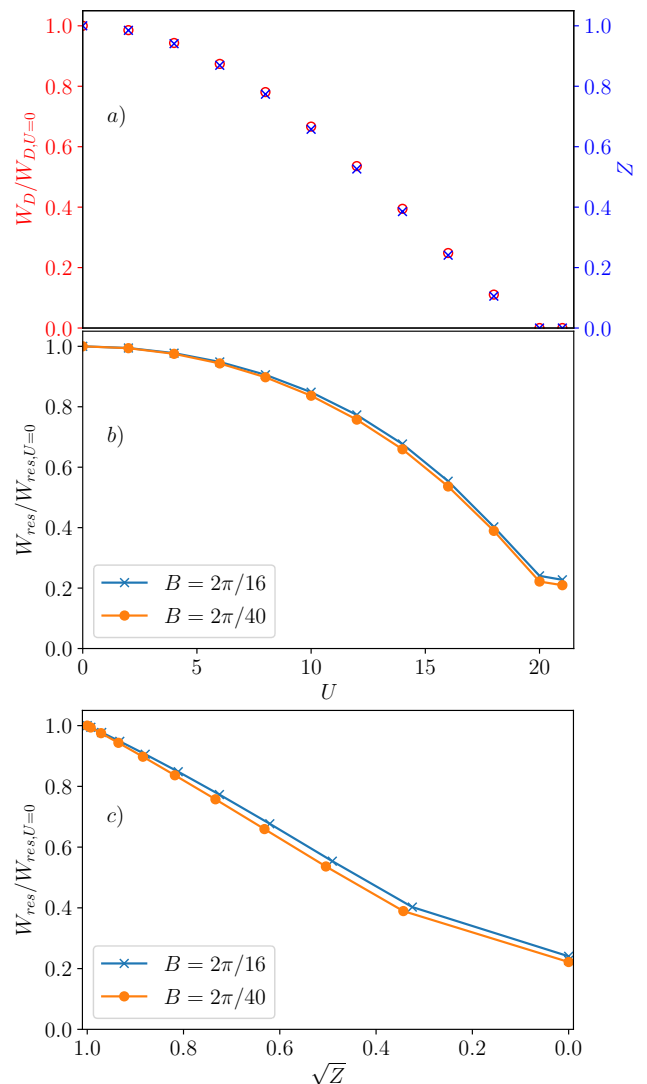


Figure 3. (color online) a) Interacting Drude-peak weight normalized by the non-interacting one (left vertical axis) and quasi-particle weight for  $B = 2\pi/16$  (right vertical axis) both as a function of interaction strength. Both quantities show identical interaction dependence. b) Spectral weight of the Drude peak normalized by the interband spectral weight as a function of  $U$ , calculated using Eq. 14. c) Normalized  $W_{res}$  as a function of square root of the quasiparticle weight  $\sqrt{Z}$  that suggests  $Z^{1/2}$  dependence. For all panels,  $\beta = 80$ .

magnetoresistance phenomenon, which is a consequence of the quantum limit where only the chiral Landau levels contribute to the Drude peak<sup>4</sup>. As one can see from Fig. 4, the linear dependence of the conductivity is not impacted by the interaction but the slope decreases upon increasing  $U$ . At higher  $U$ , the system undergoes a phase transition to a Mott phase with zero DC conductivity. Electron-electron interactions do not destroy the negative magnetoresistance, they only renormalize it, as expected from the quasiparticle picture. This statement finds its experimental proof since Weyl physics has been observed in correlated materials.<sup>7</sup>

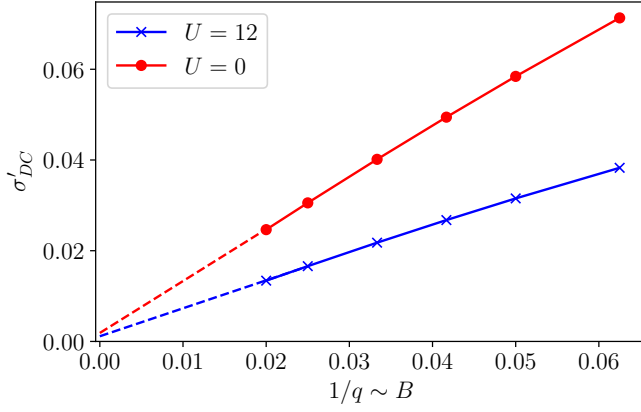


Figure 4. DC conductivity of an interacting Weyl semimetal at  $\beta = 80$  as a function of the external magnetic field. Conductivity is linearly increasing upon increasing the field strength. The slope depends on the interaction strength and decreases when  $U$  increases. The dashed parts are linear extrapolation based on the first three values of the DC conductivity.

### B. Temperature effects

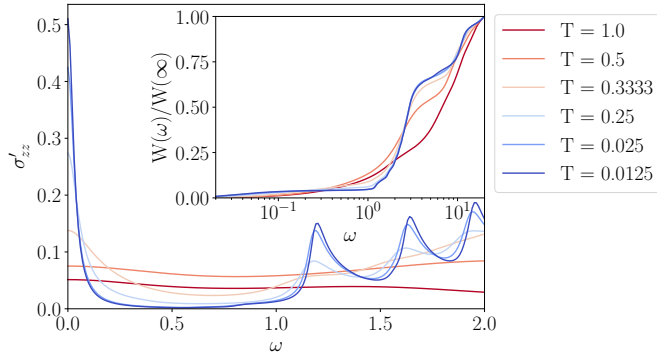


Figure 5. (color online) Magneto-optical conductivity of an interacting Weyl semimetal for several temperatures at  $B = 2\pi/40$  and  $U = 12$ . The inset shows the magneto-optical spectral weight  $W(\omega)$  as a function of cutoff frequency (cf. Eq. 15). Three distinct plateaux corresponding to the three features discussed in IV A can be seen in the inset

Bad metal behavior is a consequence of interactions.<sup>21,22,42</sup> In a Fermi liquid (FL) the crossover between a coherent metal and a bad metal can be identified from the frequency dependence of the optical conductivity at low frequencies<sup>22</sup>. At low- $T$ , the Drude peak of a FL decays as  $1/\omega^2$ . The crossover out of the FL regime leads to a broader low-frequency peak whose frequency dependence is no longer  $1/\omega^2$ . At the transition to the bad metal regime the Drude and interband features merge.<sup>22</sup> Similar behavior can be seen in the optical conductivity of a Weyl semimetal. At low- $T$ , the Drude peak is separated from the interband contribution and it decays very quickly with frequency. At higher temperatures though, both Drude peak and interband contributions broaden

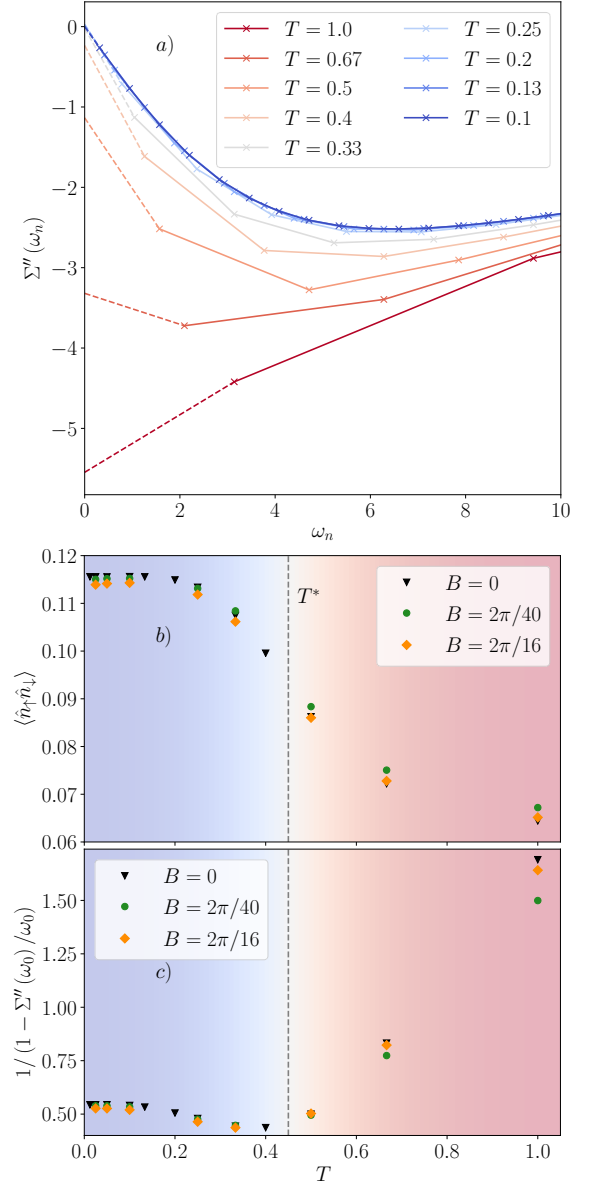


Figure 6. (color online) a) Imaginary part of the self-energy as a function of Matsubara frequencies for different temperatures.  $U$  is fixed to 12 and the system is at half-filling. The continuous lines are computed using DMFT. The dashed lines are a zero frequency extrapolation of the self-energies based on a fourth-order polynomial fit of the first five values of the self-energy. At low temperature, the self-energy extrapolates to zero like in ordinary metals. However, at higher temperature, it extrapolates to a value far from being zero at zero frequency. b) Double occupancy as a function of temperature for  $U = 12$  and for several magnetic fields.  $T^*$  can be defined by the inflection point around 0.45, marked by a vertical dashed line. c)  $T^*$  coincides with the minimum in the approximation  $(1 - \text{Im}\Sigma(\omega_0)/\omega_0)^{-1}$  for the single-particle spectral weight  $Z$ . Values of  $(1 - \text{Im}\Sigma(\omega_0)/\omega_0)^{-1}$  larger than unity are not physical and in fact quasiparticles disappear in the regime where there is an increase after reaching a minimum.

and merge together as one can see from Fig. 5 for large in-

interaction, here  $U = 12$  equal to the non-interacting bandwidth.

In fact, the merging of the Drude peak with inter-band transitions is just one of the manifestations of what happens on much larger energy scales. Indeed, the crossover affects the optical conductivity on all frequency scales. To illustrate this, we calculated the optical spectral weight integrated up to a cutoff  $\omega$

$$W(\omega) = \int_0^\omega d\nu \sigma'_{zz}(\nu), \quad (15)$$

and we plotted it as an inset in Fig. 5. At low temperatures, three frequency ranges can be identified: the Drude weight for  $\omega \in [0, 1]$  followed by the intraband contributions and finally the Hubbard band contributions at higher energies. This three-part structure is unchanged until the crossover between metal and bad metal occurs at  $T^*$ . Above  $T^*$ , the Drude and finite frequency features merge. That temperature affects dynamical properties over scales much larger than thermal energies is characteristic of strongly correlated systems.

In bad metals, the quasi-particles become ill-defined. This can be seen from the quasi-particles scattering rate, given by the imaginary part of the self-energy on the real axis. At low enough temperature, it can be approximated by the imaginary part of the Matsubara self-energy using

$$Z \approx \left(1 - \frac{\Sigma''(\omega_0)}{\omega_0}\right)^{-1}. \quad (16)$$

In Fig. 6a, the continuous lines represent the value of the self-energy obtained from DMFT for  $U = 12$  and at different temperatures. The dashed lines represent a zero frequency extrapolation based on a fourth order polynomial fit of the first five values of the self-energy. It extrapolates to zero frequency at low temperature, consistent with existence of the low-energy well-defined excitations, but at higher temperature this behavior is no longer observed.

The crossover temperature can be identified clearly from static quantities as well. Consider double occupancy, shown in Fig. 6b. The crossover temperature is around the inflection point of these curves at  $T^* \approx 0.45$ , consistent with the optical conductivity. Moreover, we also find that the crossover temperature in the presence of a magnetic field is very close to the crossover temperature obtained without magnetic field. This is because, as shown for example in Ref. 22, the bandwidth and  $U$  are clearly the two energies that control  $T^*$ . The energies associated with the magnetic fields that we consider are small compared with the bandwidth and with  $U$ , and are thus not very relevant.

The crossover can also be seen from the temperature dependence of  $(1 - \text{Im}\Sigma(\omega_0)/\omega_0)^{-1}$ , plotted at the lower panel of the Fig. 6c. At low- $T$ , this quantity gives the quasi-particle  $Z$ . As one can see, it reaches a minimum around  $T^* \approx 0.45$  and becomes even larger than unity at high enough temperature. This behavior is not physical and coincides with the disappearance of quasi-particles.

## V. CONCLUSION

In summary, our study reveals that an interacting Weyl semimetal is extremely robust to short-range interactions. The density of states at the Fermi level coming from the magnetic-field-induced chiral level is not modified by interactions. Interactions are manifest mostly through a quasiparticle renormalization  $Z$ , as in a Fermi liquid, but with a frequency-dependent self-energy that vanishes much faster with frequency as one approaches the Fermi level. The slope of the negative magnetoresistance dependence on the field is reduced by  $Z$ . At elevated temperatures, Weyl liquids exhibit a crossover to a bad metal phase at a crossover temperature that is essentially magnetic-field independent.

## ACKNOWLEDGMENTS

This work has been supported by the Natural Sciences and Engineering Research Council of Canada (NSERC) under Grant No. RGPIN-2014-04584, by the Research Chair in the Theory of Quantum Materials, by the Canada First Research Excellence Fund and by the Canadian Institute for Advanced Research. Simulations were performed on computers provided by the Canadian Foundation for Innovation, the Ministère de l'Éducation des Loisirs et du Sport (Québec), Calcul Québec, and Compute Canada.

### Appendix A: Effect of the Zeeman term on the magneto-optical conductivity

In this Appendix, we show that even unrealistically large values of the Zeeman term  $h$  do not appreciably change the magneto-optical spectrum, even though the Landau levels can be strongly modified. Fundamentally, this comes from selection rules and correlated changes of the eigenenergies in the valence and conduction bands.

We start with the weak magnetic-field case  $B = 2\pi/40$  and then consider in more detail a stronger field,  $B = 2\pi/16$  where lattice effects are more apparent and modifications of the magneto-optical conductivity more noticeable. We close by studying the case where the Zeeman term is so strong that there is a topological transition from four to two Weyl nodes. Even though we restrict ourselves to the non-interacting case, it suffices to keep in mind the quasiparticle picture, Hubbard bands and Mott transition to guess the qualitative effects of interactions.

It has been shown in Ref. 26 that, for our model, the Weyl nodes remain at  $\mu = 0$  even when  $h$  differs from zero. The Landau levels for  $B = 2\pi/40$  and  $h = 0$  appear in Fig. 7. The corresponding magneto-optical conductivity for three values of the Zeeman term,  $h = 0, 0.5, 1$ , is in Fig. 8. We already know from the density of states in the non-interacting case, Fig. 1a, that when  $h = 0$ , lattice effects become important only around  $\omega \sim \pm 2$ . This



explains why the spectrum is essentially independent of  $h$  for frequency less than about  $\omega = 4$ . Indeed, adding a Zeeman term to the Hamiltonian in Eq. (5) of Ref. 11 shows that, in the continuum model, the Zeeman term only shifts the Weyl nodes in the  $k_z$  direction without changing the energy spectrum.

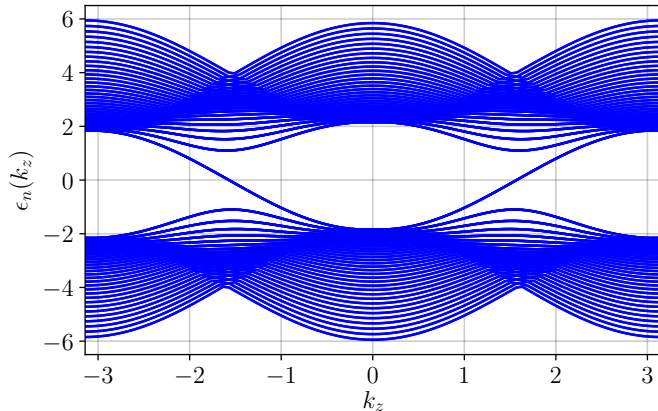


Figure 7. Landau levels for  $B = 2\pi/40$ ,  $h = 0$

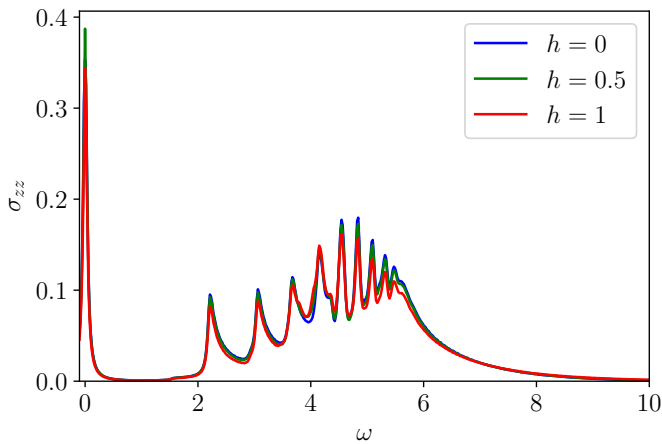


Figure 8. Magneto-optical spectrum for  $B = 2\pi/40$ ,  $h = 0, 0.5, 1$ . It is only at the highest energies that small changes can be detected. In the low-energy limit, up to  $\omega \sim 4$ , one can understand the lack to  $h$  dependence from the continuum model.

Fig. 9 shows the density of states for larger magnetic field,  $B = 2\pi/16$ , and for three values of the Zeeman field  $h = 0, 0.5, 1$ . The Landau levels are shown with the corresponding colors in Fig. 10. The difference between the three cases is striking. Note also that the magnetic field is so strong that lattice effects, as measured by the deviation from  $\omega^2$  dependence of the density of states, appear at lower frequency for the largest Zeeman term. Nevertheless, the magneto-optical spectrum, shown in Fig. 11 is not very dependent on  $h$ . Landau levels in the conduction and valence band vary in synchrony and selection rules enforce this near  $h$  independence of the spectrum, even though lattice effects are more noticeable

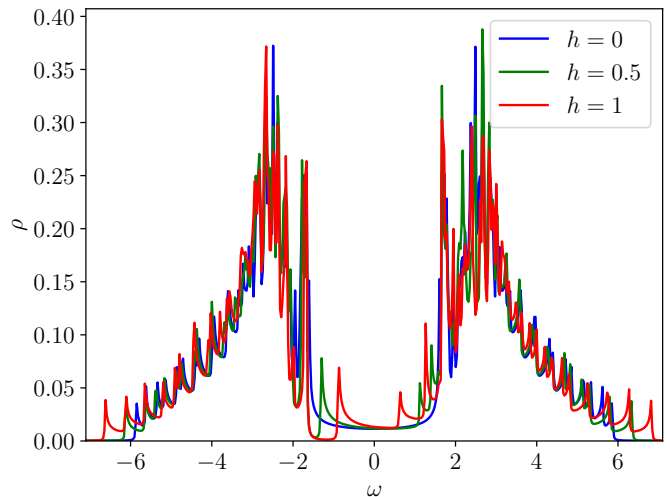


Figure 9. Local density of states for  $B = 2\pi/16$  and three values of the Zeeman term,  $h = 0, 0.5, 1$ .

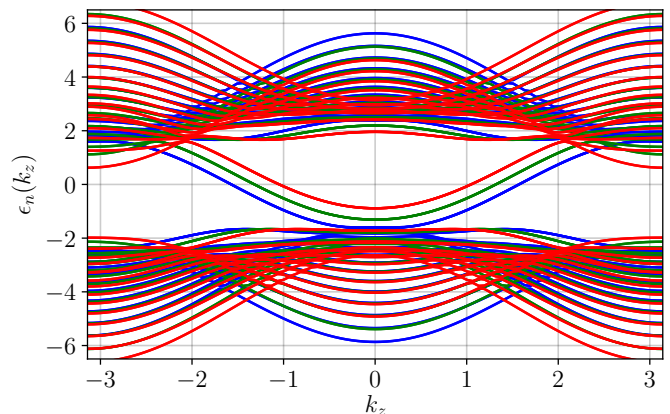


Figure 10. Landau levels for  $B = 2\pi/16$ , and  $h = 0, 0.5, 1$  with the colors corresponding to the previous figure.

than for lower  $B$  fields. Compared with  $B = 2\pi/40$ , the weight of the interband transitions has decreased compared with the Drude peak and deviations from the continuum model appear at lower frequency.

Finally, consider the extreme case near  $h = 2$  where there is a topological transition from four to two Weyl nodes. The results for the magneto-optical conductivity are in Fig. 12. While there is clearly a difference between  $h = 0$  and  $h = 1.9$ , the change across the transition, from  $h = 1.9$  to  $h = 2.1$ , is barely noticeable.

## Appendix B: Perturbation theory of the Self-energy in the DMFT framework

In order to obtain Eq. 9, we use second order perturbation theory for the self-energy. The latter is given by

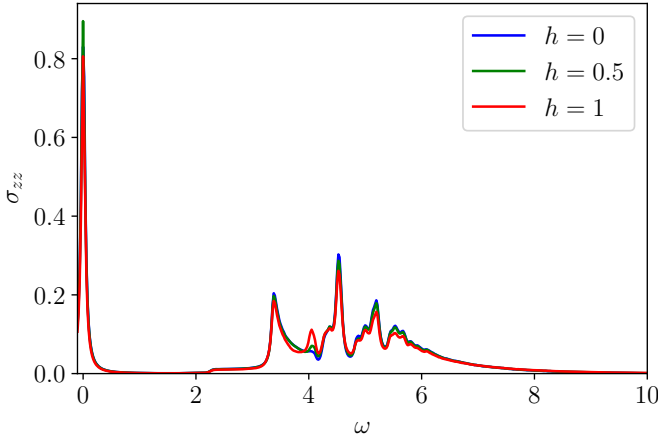


Figure 11. Magneto-optical conductivity for  $B = 2\pi/16$  and three values of the Zeeman term,  $h = 0, 0.5, 1$ . Even though the Landau levels are very different for different values of  $h$ , the magneto-optical conductivity is not very sensitive to  $h$ .

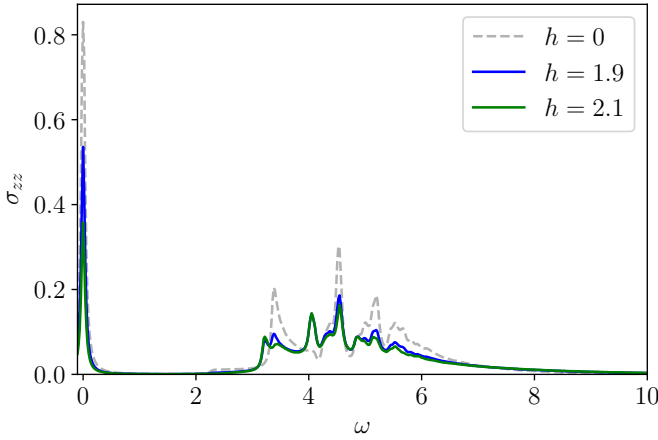


Figure 12. Magneto-optical conductivity for  $B = 2\pi/16$  and three values of the Zeeman term,  $h = 0, 1.9, 2.1$ . There is a topological transition from four to two Weyl nodes at  $h = 2$ , but nevertheless, the spectrum does not change much across the transition.

the formula:

$$\Sigma''_{\omega}(\omega) = -\pi U^2 \int_{-\omega}^0 d\epsilon_1 \int_0^{\omega+\epsilon_1} d\epsilon_2 \rho(\epsilon_1) \rho(\epsilon_2) \rho(\omega+\epsilon_1-\epsilon_2), \quad (\text{B1})$$

where  $\rho$  is the non-interacting local density of state of the impurity. This is justified in the limit  $U \rightarrow 0$ . Using the density of states of the low-energy Hamiltonian of a Weyl semimetal

$$\rho(\epsilon) = \frac{\epsilon^2}{2\pi^2 v_F^3} \quad (\text{B2})$$

leads to formula 9, which shows that the imaginary part of the self-energy scales like  $\omega^8$ .

It seems that the zero-temperature Weyl semi-metal is a sort of "super Fermi liquid" with an imaginary part

that is even smaller than the  $\omega^2$  of a Fermi liquid. Nevertheless, there is a quasiparticle spectral weight that is smaller than unity, as in Fermi-liquid theory. To show this, start from the Kramers-Kronig relations imaginary parts of self-energy

$$\Sigma'(\omega) = \mathcal{P} \int \frac{d\tilde{\omega}}{\pi} \frac{\Sigma''(\tilde{\omega})}{\tilde{\omega} - \omega}, \quad (\text{B3})$$

where  $\mathcal{P}$  stands for Cauchy's principal value. We can solve this Eq. B3 by using the identity

$$\Sigma'(\omega) = \mathcal{P} \int \frac{d\tilde{\omega}}{\pi} \frac{\Sigma''(\tilde{\omega}) - \Sigma''(\omega)}{\tilde{\omega} - \omega} + \Sigma''(\omega) \mathcal{P} \int \frac{d\tilde{\omega}}{\pi} \frac{1}{\tilde{\omega} - \omega}. \quad (\text{B4})$$

Noting that

$$\tilde{\omega}^8 - \omega^8 = (\tilde{\omega} - \omega)(\tilde{\omega} + \omega)(\tilde{\omega}^2 + \omega^2)(\tilde{\omega}^4 + \omega^4) \quad (\text{B5})$$

and using a particle-hole symmetric model, we find

$$\Sigma'(\omega) = -\frac{U^2}{40320\pi^6 v_F^9} \left( \frac{2D^7\omega}{7} + \frac{2D^5\omega^3}{5} + \frac{2D^3\omega^5}{3} + 2D\omega^7 - \omega^8 \ln\left(\left|\frac{\omega - D}{\omega + D}\right|\right) \right) \quad (\text{B6})$$

with  $D$  the bandwidth of our toy model. Equation B6 has a term linear in frequency that dominates at low frequency, other terms being of higher order in  $(\omega/D)^2$ . This behavior affects the quasiparticle weight the same way as in Fermi liquid theory since

$$Z^{-1} = 1 - \left. \frac{\partial \Sigma'(\omega)}{\partial \omega} \right|_{\omega=0}. \quad (\text{B7})$$

This proof can clearly be generalized to models without particle-hole symmetry and for  $\Sigma''(\omega) \sim -\omega^n$  with  $n$  an arbitrary integer because  $(\tilde{\omega} - \omega)$  is always a factor of  $(\tilde{\omega}^n - \omega^n)$ .

### Appendix C: Derivation of the Drude weight

Here we show how the Drude Weight can be extracted from the imaginary-frequency results for  $\Pi_{zz}(i\nu_n)$ . Taking advantage of the fact that there is a gap in the optical conductivity, we can write it as a sum of Drude and of other contributions:

$$\sigma'_{zz} = \sigma_{zz}^D + \sigma_{zz}^{res}. \quad (\text{C1})$$

Using gauge invariance, the f-sum rule<sup>43</sup> can be written as follows

$$\begin{aligned} \int d\omega \sigma'_{zz}(\omega) &= \int d\omega \sigma_{zz}^D(\omega) + \int d\omega \sigma_{zz}^{res}(\omega) \\ &= \int d\omega \frac{\Pi''_{zz}(\omega)}{\omega} = \pi \Pi_{zz}^{para}(i\nu_n = 0), \end{aligned} \quad (\text{C2})$$

where  $\Pi_{zz}^{para}$  is the paramagnetic contribution.

In Weyl semimetals subject to an external magnetic field, a selection rule on the conductivity along the direction of the magnetic field applies, as can be deduced from Ref. 11. Indeed, with  $n$  being the index of the  $n^{\text{th}}$  Landau, the only possible transitions are  $-|n| \rightarrow |n|$ . Then the contribution to the conductivity of the zeroth Landau level appears only very near zero frequency. This selection rule allows us to do a gedanken experiment and imagine that the zeroth Landau level is not present anymore. Then the f-sum rule becomes

$$\int d\omega \sigma^{\text{res}}(\omega) = \pi \tilde{\Pi}_{zz}^{\text{para}}(i\nu_n = 0), \quad (\text{C3})$$

with  $\tilde{\Pi}_{zz}^{\text{para}}(i\nu_n = 0)$  the *paramagnetic part of the correlation function in the absence of the Drude contribution*. In the absence of this contribution, there is a gap in the

optical conductivity, so the spectral representation

$$\tilde{\Pi}_{zz}^{\text{para}}(i\nu_n) = \int \frac{d\omega}{\pi} \frac{\Pi_{zz}^{\text{no Drude}}(\omega)}{\omega - i\nu_n} \quad (\text{C4})$$

tells us that at temperatures smaller than the gap,  $\tilde{\Pi}_{zz}^{\text{para}}(i\nu_n)$  can be extrapolated to  $\nu_n = 0$  from a polynomial fit of  $\Pi_{zz}^{\text{para}}(i\nu_n \neq 0)$ . Once  $\tilde{\Pi}_{zz}^{\text{para}}$  is computed, the Drude weight is easily obtained using Eq. C2

$$\int d\omega \sigma_{zz}^D(\omega) = \pi \left( \Pi_{zz}^{\text{para}}(i\nu_n = 0) - \tilde{\Pi}_{zz}^{\text{para}}(i\nu_n = 0) \right). \quad (\text{C5})$$

Given the remarkable robustness of quasiparticle physics in Weyl semimetal at low temperature, we can use this result even for large values of  $U$ , as long as there is a gap between the Drude peak and the interband transitions.

- 
- <sup>1</sup> Davide Grassano, Olivia Pulci, Adriano Mosca Conte, and Friedhelm Bechstedt, “Validity of weyl fermion picture for transition metals mononictides taas, tap, nbas, and nbp from ab initio studies,” *Scientific Reports* **8**, 3534 (2018).
  - <sup>2</sup> Hongming Weng, Chen Fang, Zhong Fang, B. Andrei Bernevig, and Xi Dai, “Weyl semimetal phase in non-centrosymmetric transition-metal monophosphides,” *Phys. Rev. X* **5**, 011029 (2015).
  - <sup>3</sup> Chi-Cheng Lee, Su-Yang Xu, Shin-Ming Huang, Daniel S. Sanchez, Ilya Belopolski, Guoqing Chang, Guang Bian, Nasser Alidoust, Hao Zheng, Madhab Neupane, Baokai Wang, Arun Bansil, M. Zahid Hasan, and Hsin Lin, “Fermi surface interconnectivity and topology in weyl fermion semimetals taas, tap, nbas, and nbp,” *Phys. Rev. B* **92**, 235104 (2015).
  - <sup>4</sup> D. T. Son and B. Z. Spivak, “Chiral anomaly and classical negative magnetoresistance of weyl metals,” *Phys. Rev. B* **88**, 104412 (2013).
  - <sup>5</sup> Shin-Ming Huang, Su-Yang Xu, Ilya Belopolski, Chi-Cheng Lee, Guoqing Chang, BaoKai Wang, Nasser Alidoust, Guang Bian, Madhab Neupane, Chenglong Zhang, Shuang Jia, Arun Bansil, Hsin Lin, and M. Zahid Hasan, “A weyl fermion semimetal with surface fermi arcs in the transition metal mononictide taas class,” *Nature Communications* **6**, 7373 (2015).
  - <sup>6</sup> Cheng-Long Zhang, Su-Yang Xu, Ilya Belopolski, Zhujun Yuan, Ziquan Lin, Bingbing Tong, Guang Bian, Nasser Alidoust, Chi-Cheng Lee, Shin-Ming Huang, Tay-Rong Chang, Guoqing Chang, Chuang-Han Hsu, Horng-Tay Jeng, Madhab Neupane, Daniel S. Sanchez, Hao Zheng, Junfeng Wang, Hsin Lin, Chi Zhang, Hai-Zhou Lu, Shun-Qing Shen, Titus Neupert, M. Zahid Hasan, and Shuang Jia, “Signatures of the adler-bell-jackiw chiral anomaly in a weyl fermion semimetal,” *Nature Communications* **7**, 10735 (2016).
  - <sup>7</sup> K. Kuroda, T. Tomita, M.-T. Suzuki, C. Bareille, A. ?. A. Nugroho, P. Goswami, M. Ochi, M. Ikhlas, M. Nakayama, S. Akebi, R. Noguchi, R. Ishii, N. Inami, K. Ono, H. Kumigashira, A. Varykhalov, T. Muro, T. Koretsune, R. Arita, S. Shin, Takeshi Kondo, and S. Nakatsuji, “Evidence for magnetic weyl fermions in a correlated metal,” *Nature Materials* **16**, 1090 EP – (2017).
  - <sup>8</sup> Frank Arnold, Chandra Shekhar, Shu-Chun Wu, Yan Sun, Ricardo Donizeth dos Reis, Nitesh Kumar, Marcel Naumann, Mukkattu O. Ajeesh, Marcus Schmidt, Adolfo G. Grushin, Jens H. Bardarson, Michael Baenitz, Dmitry Sokolov, Horst Borrmann, Michael Nicklas, Claudia Felser, Elena Hassinger, and Binghai Yan, “Negative magnetoresistance without well-defined chirality in the weyl semimetal tap,” *Nature Communications* **7**, 11615 (2016).
  - <sup>9</sup> Pallab Goswami, J. H. Pixley, and S. Das Sarma, “Axial anomaly and longitudinal magnetoresistance of a generic three-dimensional metal,” *Phys. Rev. B* **92**, 075205 (2015).
  - <sup>10</sup> M. Naumann, F. Arnold, M. D. Bachmann, K. A. Modic, P. J. W. Moll, V. Suss, M. Schmidt, and E. Hassinger, “Orbital effect and weak localization in the longitudinal magnetoresistance of weyl semimetals nbp, nbas, tap, and taas,” *Physical Review Materials* **4**, 034201 (2020).
  - <sup>11</sup> Phillip E. C. Ashby and J. P. Carbotte, “Magneto-optical conductivity of weyl semimetals,” *Phys. Rev. B* **87**, 245131 (2013).
  - <sup>12</sup> Seongjin Ahn, E. J. Mele, and Hongki Min, “Optical conductivity of multi-Weyl semimetals,” *Physical Review B* (2017), 10.1103/PhysRevB.95.161112, arXiv:1609.08566.
  - <sup>13</sup> B. Xu, Y. M. Dai, L. X. Zhao, K. Wang, R. Yang, W. Zhang, J. Y. Liu, H. Xiao, G. F. Chen, A. J. Taylor, D. A. Yarotski, R. P. Prasankumar, and X. G. Qiu, “Optical spectroscopy of the weyl semimetal taas,” *Phys. Rev. B* **93**, 121110 (2016).
  - <sup>14</sup> Xiang Yuan, Zhongbo Yan, Chaoyu Song, Mengyao Zhang, Zhilin Li, Cheng Zhang, Yanwen Liu, Weiyi Wang, Minhao Zhao, Zehao Lin, and et al., “Chiral landau levels in weyl semimetal nbas with multiple topological carriers,” *Nature Communications* **9**, 1854 (2018).
  - <sup>15</sup> Yuxuan Jiang, Zhiling Dun, Seonghill Moon, Haidong Zhou, Mikito Koshino, Dmitry Smirnov, and Zhigang Jiang, “Landau quantization in coupled weyl points: A case study of semimetal nbp,” *Nano Letters* **18**, 7726–7731 (2018), pMID: 30403143, <https://doi.org/10.1021/acs.nanolett.8b03418>.
  - <sup>16</sup> Simon Bertrand, Jean-Michel Parent, René Côté, and Ion Garate, “Complete optical valley polarization in weyl

- semimetals in strong magnetic fields,” *Phys. Rev. B* **100**, 075107 (2019).
- <sup>17</sup> Antoine Georges, Gabriel Kotliar, Werner Krauth, and Marcelo J. Rozenberg, “Dynamical mean-field theory of strongly correlated fermion systems and the limit of infinite dimensions,” *Rev. Mod. Phys.* **68**, 13–125 (1996).
- <sup>18</sup> Shaheen Acheche, *Effets des corrélations électroniques et du champ magnétique dans les semi-métaux de Weyl*, Ph.D. thesis, Université de Sherbrooke, Sherbrooke (2019).
- <sup>19</sup> Bitan Roy, Robert-Jan Slager, and Vladimir Juričić, “Global phase diagram of a dirty weyl liquid and emergent superuniversality,” *Phys. Rev. X* **8**, 031076 (2018).
- <sup>20</sup> AF Ioffe and AR Regel, “Non-crystalline, amorphous and liquid electronic semiconductors,” *Prog. Semicond* **4**, 237–291 (1960).
- <sup>21</sup> Peter T. Brown, Debayan Mitra, Elmer Guardado-Sanchez, Reza Nourafkan, Alexis Reymbaut, Charles-David Hébert, Simon Bergeron, A.-M. S. Tremblay, Jure Kokalj, David A. Huse, Peter Schauß, and Waseem S. Bakr, “Bad metallic transport in a cold atom fermi-hubbard system,” *Science* **363**, 379–382 (2019).
- <sup>22</sup> Xiaoyu Deng, Jernej Mravlje, Rok Žitko, Michel Ferrero, Gabriel Kotliar, and Antoine Georges, “How bad metals turn good: Spectroscopic signatures of resilient quasiparticles,” *Phys. Rev. Lett.* **110**, 086401 (2013).
- <sup>23</sup> Wenhui Xu, Kristjan Haule, and Gabriel Kotliar, “Hidden fermi liquid, scattering rate saturation, and nernst effect: A dynamical mean-field theory perspective,” *Physical Review Letters* **111**, 036401 (2013).
- <sup>24</sup> Peter Cha, Aavishkar A. Patel, Emanuel Gull, and Eun-Ah Kim, “ $t$ -linear resistivity in models with local self-energy,” [arXiv:1910.07530 \[cond-mat\]](https://arxiv.org/abs/1910.07530) (2019), arXiv: 1910.07530.
- <sup>25</sup> Sthitadhi Roy, Michael Kolodrubetz, Joel E. Moore, and Adolfo G. Grushin, “Chern numbers and chiral anomalies in weyl butterflies,” *Phys. Rev. B* **94**, 161107 (2016).
- <sup>26</sup> S. Acheche, R. Nourafkan, and A.-M. S. Tremblay, “Orbital magnetization and anomalous hall effect in interacting weyl semimetals,” *Phys. Rev. B* **99**, 075144 (2019).
- <sup>27</sup> Mahito Kohmoto, “Topological invariant and the quantization of the hall conductance,” *Annals of Physics* **160**, 343 – 354 (1985).
- <sup>28</sup> Douglas R. Hofstadter, “Energy levels and wave functions of bloch electrons in rational and irrational magnetic fields,” *Phys. Rev. B* **14**, 2239–2249 (1976).
- <sup>29</sup> S. Acheche, L.-F. Arsenault, and A.-M. S. Tremblay, “Orbital effect of the magnetic field in dynamical mean-field theory,” *Phys. Rev. B* **96**, 235135 (2017).
- <sup>30</sup> T. Schäfer, A. Toschi, and Jan M. Tomczak, “Separability of dynamical and nonlocal correlations in three dimensions,” *Phys. Rev. B* **91**, 121107 (2015).
- <sup>31</sup> R. Nourafkan, G. Kotliar, and A.-M. S. Tremblay, “Orbital magnetization of correlated electrons with arbitrary band topology,” *Phys. Rev. B* **90**, 125132 (2014).
- <sup>32</sup> Michel Caffarel and Werner Krauth, “Exact diagonalization approach to correlated fermions in infinite dimensions: Mott transition and superconductivity,” *Physical Review Letters* **72**, 1545–1548 (1994).
- <sup>33</sup> Reza Nourafkan and Frank Marsiglio, “Surface effects in doping a mott insulator,” *Phys. Rev. B* **83**, 155116 (2011).
- <sup>34</sup> E Müller-Hartmann, “Fermions on a lattice in high dimensions,” *International Journal of Modern Physics B* **3**, 2169–2187 (1989).
- <sup>35</sup> Henrik Kajueter and Gabriel Kotliar, “New iterative perturbation scheme for lattice models with arbitrary filling,” *Physical review letters* **77**, 131 (1996).
- <sup>36</sup> G.D. Mahan, *Many-Particle Physics*, Physics of Solids and Liquids (Springer US, 2012).
- <sup>37</sup> R. Nourafkan and A.-M. S. Tremblay, “Hall and faraday effects in interacting multiband systems with arbitrary band topology and spin-orbit coupling,” *Phys. Rev. B* **98**, 165130 (2018).
- <sup>38</sup> R. Nourafkan, F. Marsiglio, and G. Kotliar, “Model of the electron-phonon interaction and optical conductivity of  $\text{ba}_{1-x}\text{k}_x\text{bio}_3$  superconductors,” *Phys. Rev. Lett.* **109**, 017001 (2012).
- <sup>39</sup> H. J. Vidberg and J. W. Serene, “Solving the eliasberg equations by means ofn-point padé approximants,” *Journal of Low Temperature Physics* **29**, 179–192 (1977).
- <sup>40</sup> N.W. Ashcroft and N.D. Mermin, *Solid State Physics*, HRW international editions (Holt, Rinehart and Winston, 1976).
- <sup>41</sup> Takahiro Morimoto and Naoto Nagaosa, “Weyl mott insulator,” *Scientific reports* **6**, 1–6 (2016).
- <sup>42</sup> N. E. Hussey, K. Takenaka, and H. Takagi, “Universality of the mott-ioffe-regel limit in metals,” *Philosophical Magazine* **84**, 2847–2864 (2004).
- <sup>43</sup> Pierre F. Maldague, “Optical spectrum of a hubbard chain,” *Phys. Rev. B* **16**, 2437–2446 (1977).